Supporting Information

Number of Surface-Attached Acceptors on a Quantum Dot Impacts Energy Transfer and Photon Upconversion Efficiencies

Jie Zhang[†], Hironori Kouno[§], Nobuhiro Yanai*[,§,∥], Daichi Eguchi[‡], Tatsuo Nakagawa[#], Nobuo Kimizuka*[,§], Toshiharu Teranishi*[,‡], and Masanori Sakamoto*[,‡]

[†]Department of Chemistry, Graduate School of Science, Kyoto University, Gokasho, Uji, Kyoto 611-0011, Japan

[‡]Institute for Chemical Research, Kyoto University, Gokasho, Uji, Kyoto 611-0011, Japan

[§]Department of Chemistry and Biochemistry, Faculty of Engineering, Center for Molecular Systems (CMS), Kyushu University, Moto-oka 744, Nishi-ku, Fukuoka 819-0395, Japan

[∥]PRESTO, JST, Honcho 4-1-8, Kawaguchi, Saitama 332-0012, Japan

[#]Optical Instruments Division, Unisoku Co., Ltd., Kasugano 2-4-3, Hirakata, Osaka 573-0131, Japan

1. Estimation of the number of Pe on a QD

The optical density (O.D.) at the first exciton peak was used to determine the QD concentration ([QD]) in the QD-Pe toluene solutions using the Beer–Lambert law,

$$\text{O.D.} = \varepsilon[\text{QD}]l \tag{S1}$$

where ε and l are the absorption coefficient of light absorbers and optical path length, respectively. We used ε of the QDs from a previous report.[1] ε of Pe was determined by concentration-dependent UV-vis measurements. We calculated [QD] from O.D. of the first exciton peak using equation 1 because Pe does not absorb light at the wavelength of the first exciton peak of the QDs. Then, the concentration of Pe ([Pe]) was calculated using O.D. of the absorption peak of Pe. Because the absorption of Pe overlapped with that of the QDs, the absorption spectrum of the QDs was subtracted from that of QD-Pe to obtain the O.D. of Pe. Finally, n was determined using equation S2,

$$n = [\text{Pe}]/[\text{QD}] \tag{S2}$$

The extinction coefficient (ε) of Pe at 455 nm in toluene was estimated to be 23500 M^{-1} cm^{-1} from concentration-dependent UV-vis measurements. The ε values of the QDs were obtained from a previous report.[1] The ε values of CdTe QDs were 125684 M^{-1} cm^{-1} at 555 nm, 157407 M^{-1} cm^{-1} at 600 nm, and 210726 M^{-1} cm^{-1} at 643 nm. The ε values of CdSe QDs were 134113 M^{-1} cm^{-1} at 560 nm, 245938 M^{-1} cm^{-1} at 588 nm, and 453554 M^{-1} cm^{-1} at 612 nm.

2. Estimation of the quantum yield of TTET

Quantum yields of TTET from QDs to Pe were estimated using the TA measurements. We show the estimation of the quantum yield for TTET of CdSe (3.3 nm)-Pe (n = 16) as an example. The quantum yield was estimated using the following equation:

$$\Phi_{TTET} = \frac{n\,[^3\mathrm{Pe}^*]}{N_{\mathrm{photons}}} \tag{S3}$$

where $n\,[^3\mathrm{Pe}^*]$ is the number of Pe (T_1) and N_{photons} is the number of photons absorbed by CdSe (3.3 nm).

N_{photons} was calculated using equation (S4):

$$N_{photons} = \frac{A \times \text{Total energy of one pulse}}{\text{Energy of single photon}}\left(1 - 10^{-O.D.560}\right) \tag{S4}$$

where A is the ratio of the beam intensity within the FWHM of a laser pulse (0.5) to the whole intensity. The total energy of one pulse was 3 μJ and the energy of a single photon was estimated using equation (S5).

$$\text{Energy of single photon} = \frac{hc}{\lambda} \tag{S5}$$

where h, c, and λ are the Plank constant (6.63×10^{-34} J·s), the speed of light (3.00×10^{8} m·s^{-1}) and the wavelength of the pump laser (560 nm), respectively. From equation (S5), the energy of a single photon was calculated to be 3.55×10^{-19} J. The O.D. of CdSe (3.3 nm)-Pe (n = 16) was 0.5 at the excitation wavelength (560 nm). Thus, N_{photons} was calculated to be 2.89×10^{12}.

Because the relaxation dynamics of CdSe QDs completed within 500 ns after excitation, the transient signal after 500 ns probed at 490 nm is almost solely derived from Pe (T_1). In addition, the intensity of Pe (T_1) does not decay markedly at 500 nm after laser excitation because of the long lifetime of Pe (T_1). Thus, the concentration of Pe (T_1) generated upon TTET from CdSe was determined using the ΔO.D. at 500 ns (0.00325) and its corresponding triplet molar absorption coefficient (ε = 14300 M^{-1} cm^{-1}).[2] The number of Pe (T_1) was determined using equation (S6):

$$n\,[^3\mathrm{Pe}^*] = \frac{\Delta\mathrm{O.D.}}{\varepsilon L}\,SLN_A \tag{S6}$$

where L, S, and N_A are the optical path length in the solution (2 mm), the spot area of the pump laser (1 mm^2), and Avogadro constant (6.02×10^{23} mol^{-1}), respectively. Thus, $n\,[^3\mathrm{Pe}^*]$ was calculated to be 1.32×10^{12}. Finally, Φ_{TTET} was determined to be 47.2%.

The quantum yields of Pe (T_1) for other samples were determined using the same procedure. The ΔO.D. of QD-Pe (T_1) at 500 nm after laser excitation was used to estimate its concentration. The obtained values are shown below:

CdSe (3.3 nm)-Pe (n = 6.0): 0.00130; CdSe (3.3 nm)-Pe (n = 9.5): 0.00196; CdSe (4.2 nm)-Pe (n = 9.3): 0.00197; CdSe (4.2 nm)-Pe (n = 18): 0.00280; CdSe (4.2 nm)-Pe (n = 38):0.00385; CdTe (3.4 nm)-Pe (n = 8.1): 0.000313; CdTe (3.4 nm)-Pe (n = 14): 0.000567; CdTe (3.4 nm)-Pe (n = 19): 0.000872; CdTe (3.7 nm)-Pe (n = 11): 0.000205; CdTe (3.7 nm)-Pe (n = 18): 0.000284; CdTe (3.7 nm)-Pe (n = 30): 0.000457.

The total energies of one pulse for CdSe (4.2 nm)-Pe, CdTe (3.4 nm)-Pe, and CdTe (3.7 nm)-Pe were 6, 0.9, and 1.6 μJ, respectively. The wavelengths of the pump laser for CdSe (4.2 nm)-Pe, CdTe (3.4 nm)-Pe, and CdTe (3.7 nm)-Pe were 590, 560, and 600 nm, respectively. The ε values of Pe-COOH (T_1) at 500 and 505 nm were calculated to be 20100 and 22000 M^{-1} cm^{-1}, respectively.

3. Estimation of the maximum number of Pe on a QD

We estimated the maximum number of Pe on a QD through geometrical considerations. Because the number of sites for molecules on a QD is restricted by the surface area of the QD, the maximum

number of Pe (n_{max}) was estimated from the surface area of QDs and size of Pe molecules using equation (S7),

$$n_{\max} = \frac{S_{\mathrm{QD}}}{S_{\mathrm{Pe}}} = (4\pi r_{\mathrm{QD}}^2)/(\pi r_{\mathrm{Pe}}^2), \tag{S7}$$

where S_{QD} is the surface area of the QD, S_{Pe} is the area occupied by one Pe molecule on a QD, r_{QD} is the radius of the QD ($r_{CdSe\ (3.3\ nm)}$ is 1.6 nm, $r_{CdSe\ (4.2\ nm)}$ is 2.1 nm, $r_{CdTe\ (3.4\ nm)}$ is 1.7 nm, and $r_{CdTe\ (3.7\ nm)}$ is 1.9 nm), and r_{Pe} is the radius of Pe (0.33 nm). The maximum numbers of Pe on CdSe (3.3 nm), CdSe (4.2 nm), CdTe (3.4 nm), and CdTe (3.7 nm) were calculated to be 94, 162, 106, and 133, respectively.

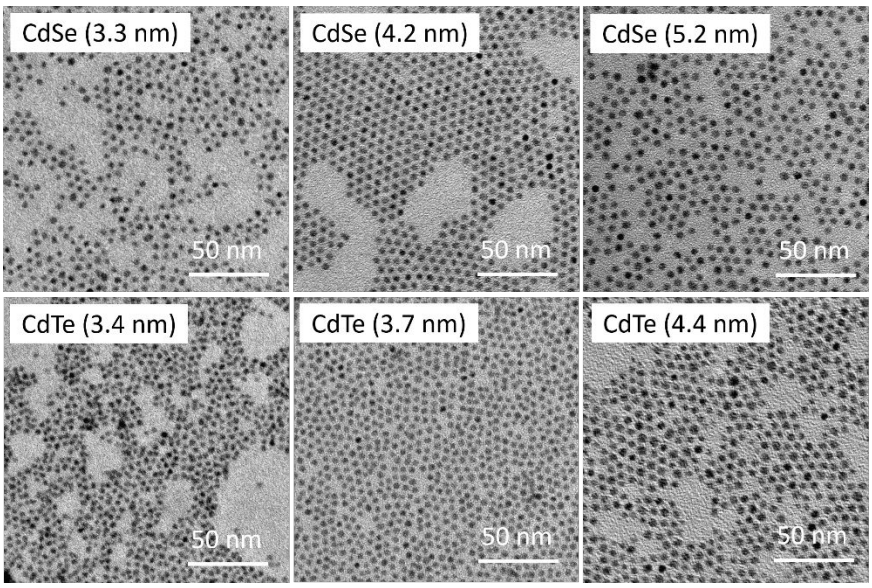

Figure S1. TEM images of QDs.

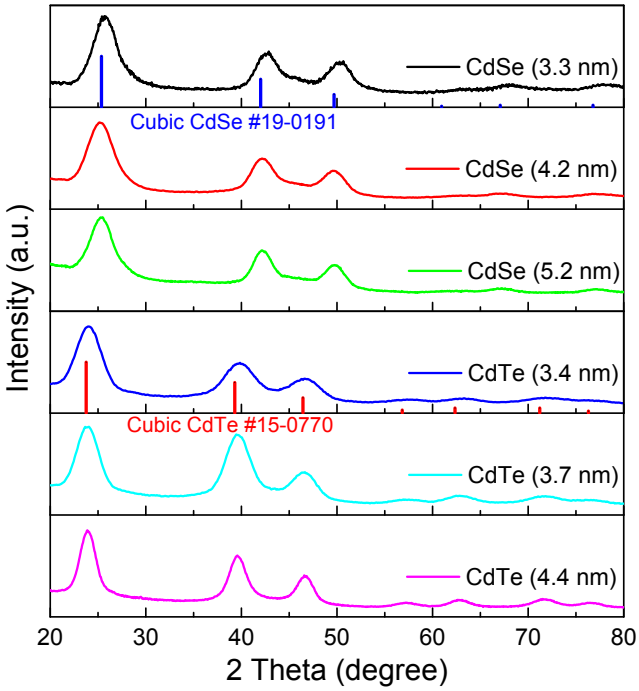

Figure S2. XRD patterns of QDs.

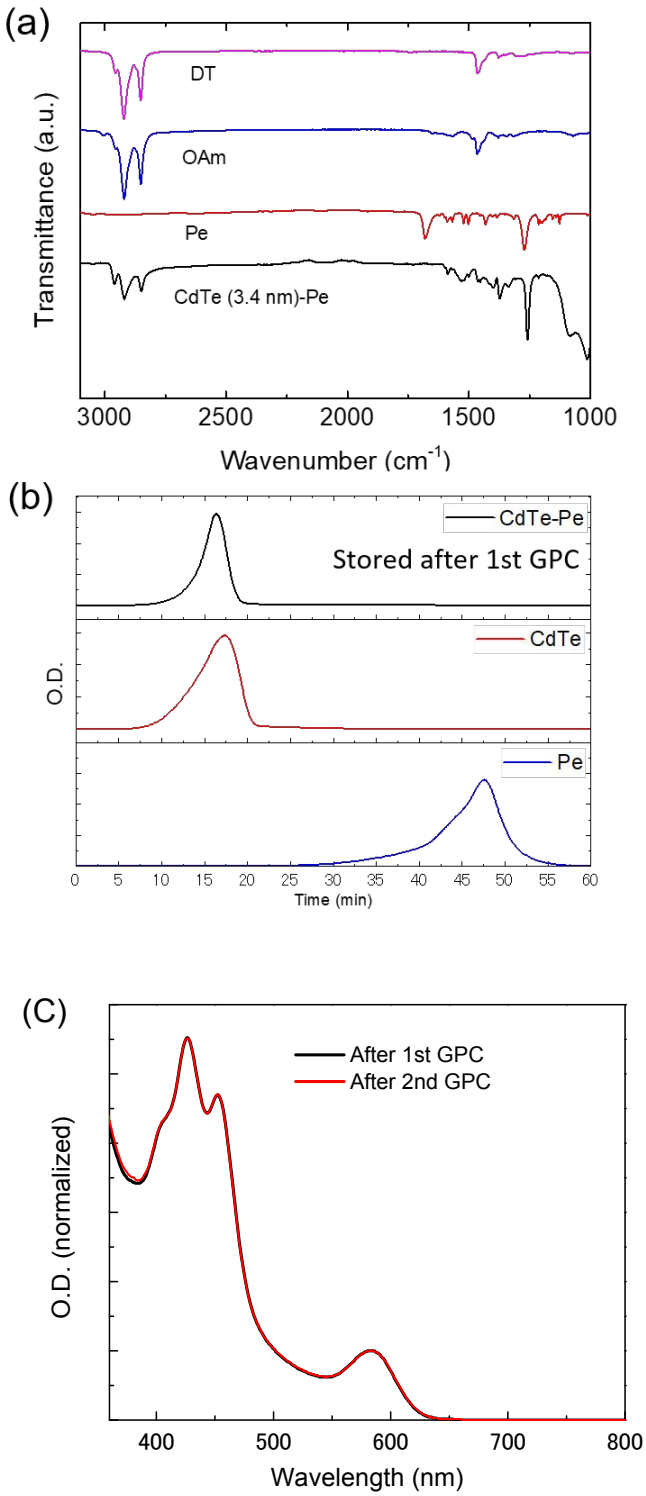

Figure S3. (a) FTIR spectra of DT, OAm, free Pe, and CdTe (3.4 nm)-Pe. (b) Measurement of GPC chromatogram of CdTe-Pe one day after the purification. (c) Normalized UV-Vis-NIR

spectra of QD-Pe just after purification by GPC (1st GPC). Normalized UV-Vis-NIR spectra of the sample solution stored for one day and purified again (2nd GPC).

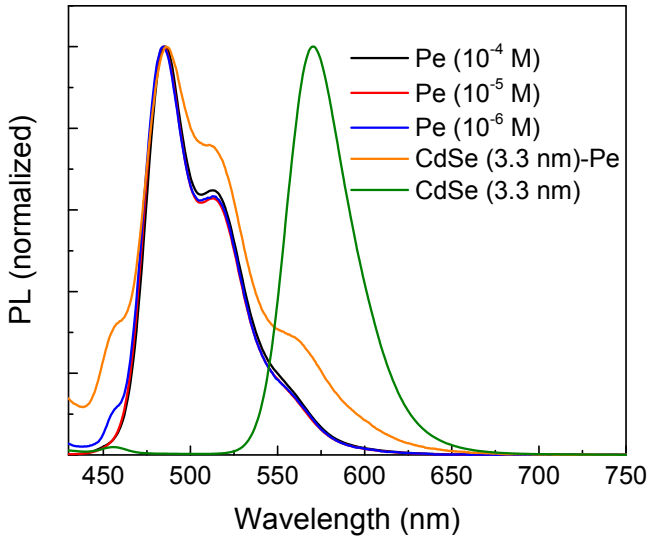

Figure S4 Normalized emission spectra of Pe with different concentrations, CdSe (3.3 nm)-Pe, and CdSe (3.3 nm) under 400 nm excitation.

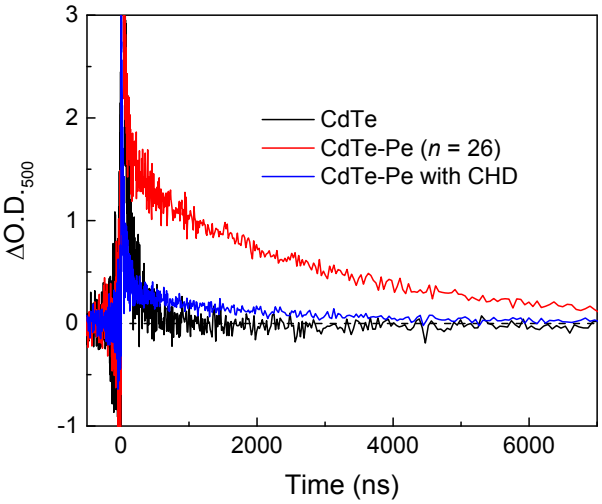

Figure S5. Kinetic profiles of CdTe-Pe (n = 26) at 500 nm in quenching experiments with or without triplet quencher. CHD: 1,4-cyclohexadiene.

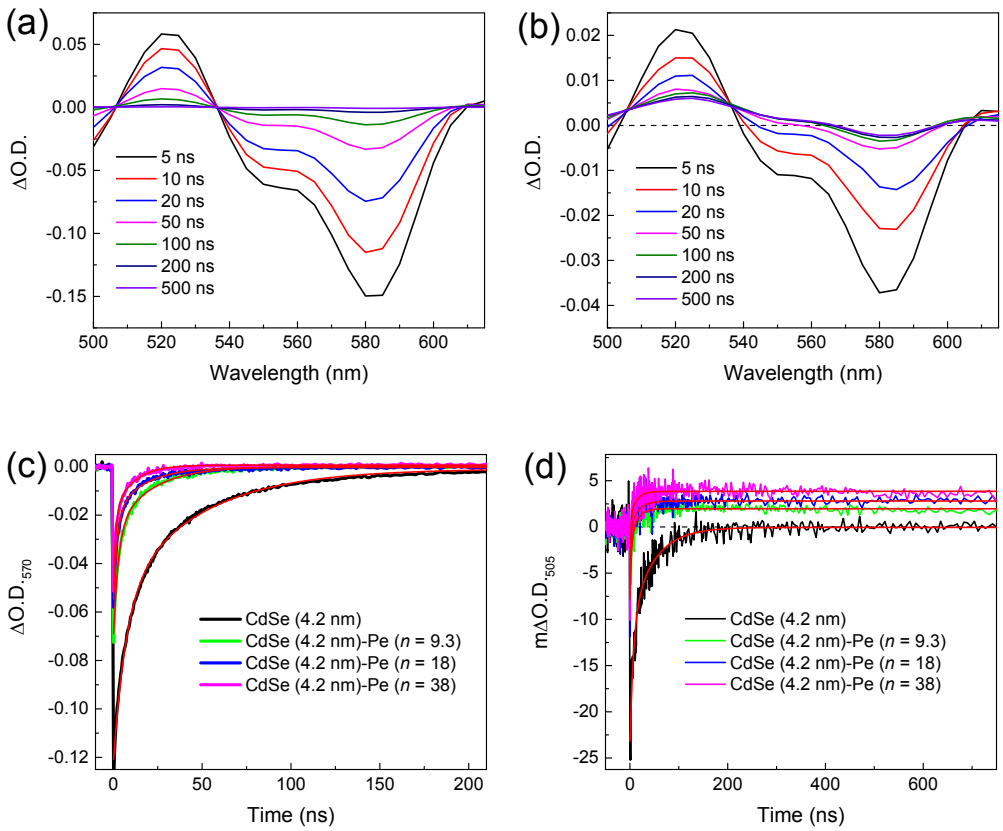

Figure S6. TA spectra of CdSe (4.2 nm)-Pe upon excitation by a 590-nm laser. TA spectra of (a) CdSe (4.2 nm) and (b) CdSe(4.2 nm)-Pe in toluene solution upon selective excitation of CdSe (3.3 nm) using 590-nm pump-laser excitation (6 μJ per pulse). (c) The ground-state bleaching of CdSe (4.2 nm) and CdSe (4.2 nm)-Pe upon 590-nm laser excitation probed at 570 nm. Solid smooth lines are the best fit. (d) Kinetic profiles at 505 nm for the growth of triplet absorption of Pe upon 590-nm laser excitation. Solid smooth lines are the best fit.

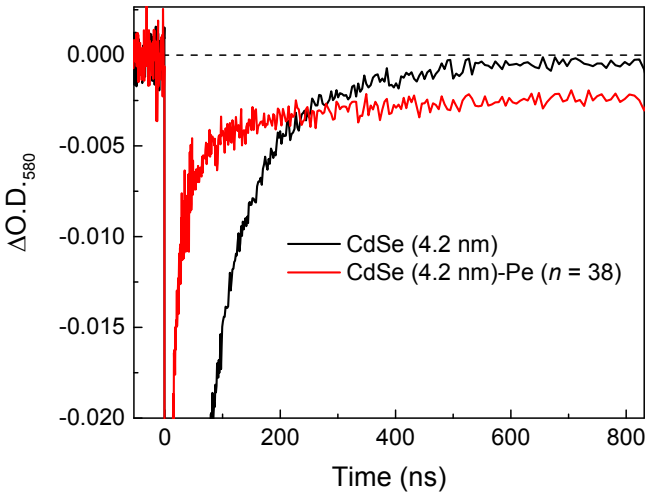

Figure S7. Kinetic profiles at 580 nm of CdSe (4.2 nm) and CdSe (4.2 nm)-Pe upon excitation by a 590-nm laser (6 μJ per pulse). Upon excitation by a 590-nm laser pulse, the recovery of the bleaching of CdSe (4.2 nm) was completed within 500 ns. In contrast, CdSe (4.2 nm)-Pe exhibited bleaching even after 500 ns, which is because of the back TTET from Pe-COOH (T_1) to CdSe (4.2 nm). Because the lifetime of Pe (T_1) is much longer than that of CdSe (4.2 nm) in the excited state (CdSe (4.2 nm)*), the back energy transfer markedly prolonged the lifetime of CdSe (4.2 nm)*, which was observed as bleaching. A similar equilibrium formation has been reported previously.[3-4]

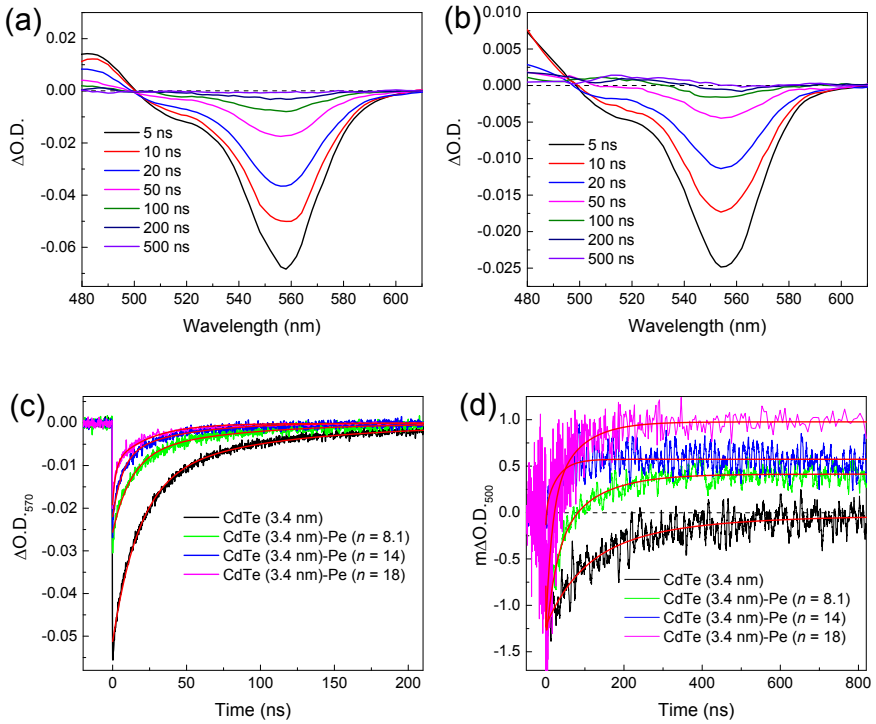

Figure S8. TA spectra of CdTe (3.4 nm)-Pe upon excitation by a 560-nm laser. TA spectra of (a) CdTe (3.4 nm) and (b) CdTe (3.4 nm)-Pe in toluene solution upon selective excitation of CdTe (3.4 nm) using 560-nm pump-laser excitation (0.9 μJ per pulse). (c) The ground-state bleaching of CdTe (3.4 nm) and CdTe (3.4 nm)-Pe upon 560-nm laser excitation probed at 570 nm. Solid smooth lines are the best fit. (d) Kinetic profiles at 500 nm for the growth of triplet absorption of Pe upon 560-nm laser excitation. Solid smooth lines are the best fit.

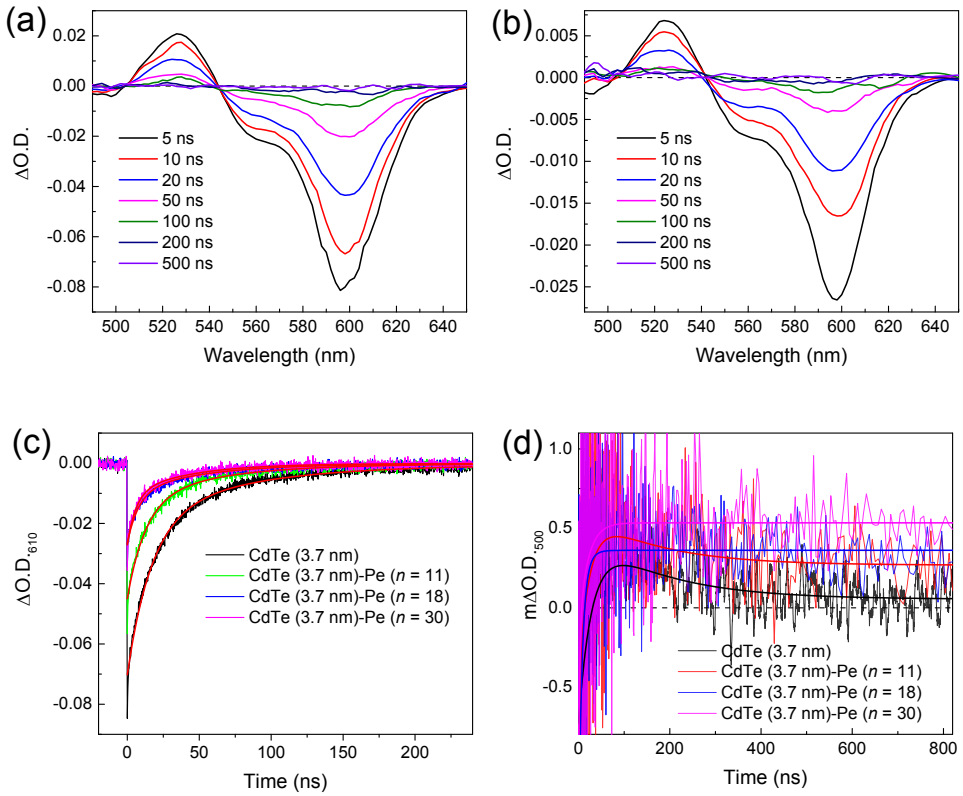

Figure S9. TA spectra of CdTe (3.7 nm)-Pe upon excitation by a 600-nm laser. TA spectra of (a) CdTe (3.7 nm) and (b) CdTe (3.7 nm)-Pe in toluene solution upon selective excitation of CdTe (3.7 nm) using 600-nm pump laser excitation (1.6 μJ per pulse). (c) Ground-state bleaching of CdTe (3.7 nm) and CdTe (3.7 nm)-Pe upon 600-nm laser excitation probed at 610 nm. Solid smooth lines are the best fit. (d) Kinetic profiles at 500 nm for the growth of triplet absorption of Pe upon 600-nm laser excitation. Solid smooth lines are the best fit.

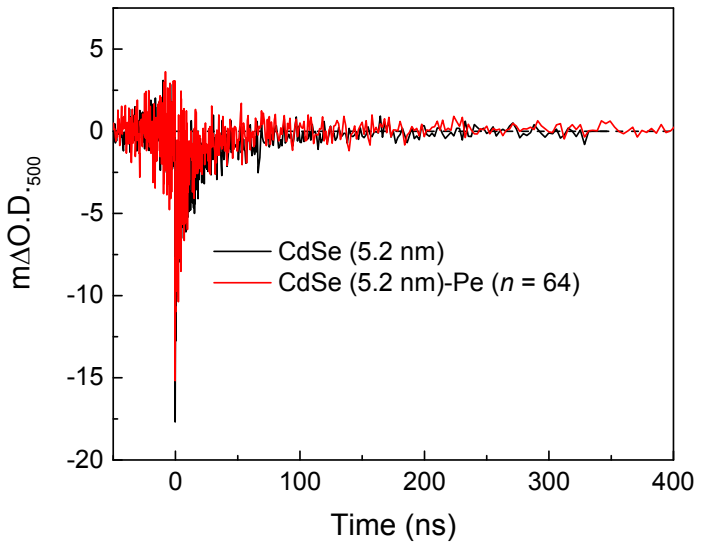

Figure S10. Kinetic profiles at 500 nm of CdSe (5.2 nm) and CdSe (5.2 nm)-Pe upon selective excitation at 620 nm (7 μJ per pulse). No TTET was observed.

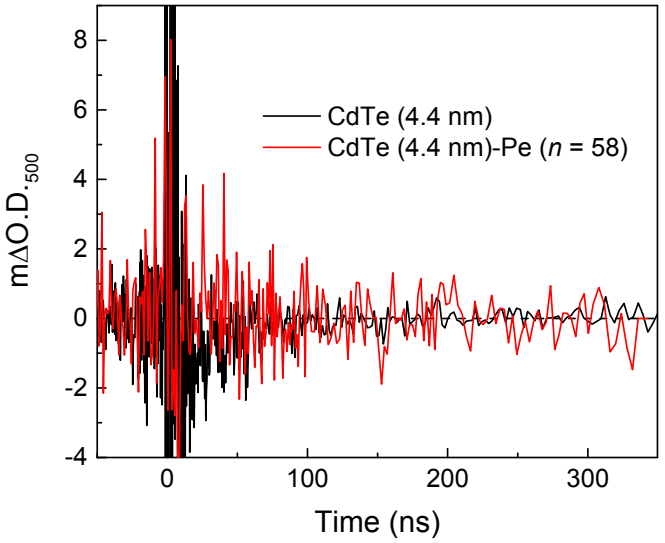

Figure S11. Kinetic profiles at 500 nm of CdTe (4.4 nm) and CdTe (4.4 nm)-Pe upon selective excitation at 650 nm (6 μJ per pulse). No TTET was observed.

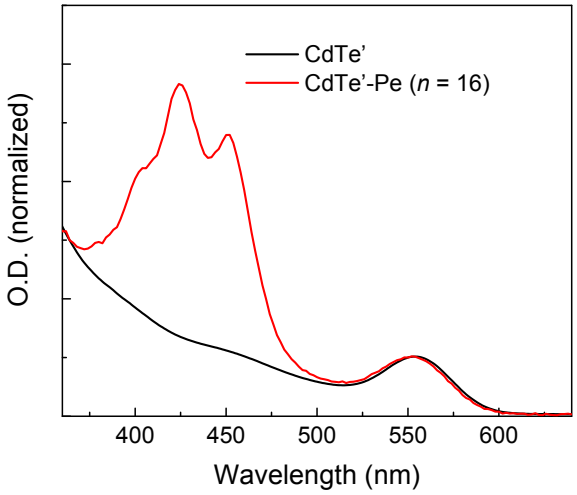

Figure S12. UV-vis spectra of CdTe' and CdTe'-Pe.

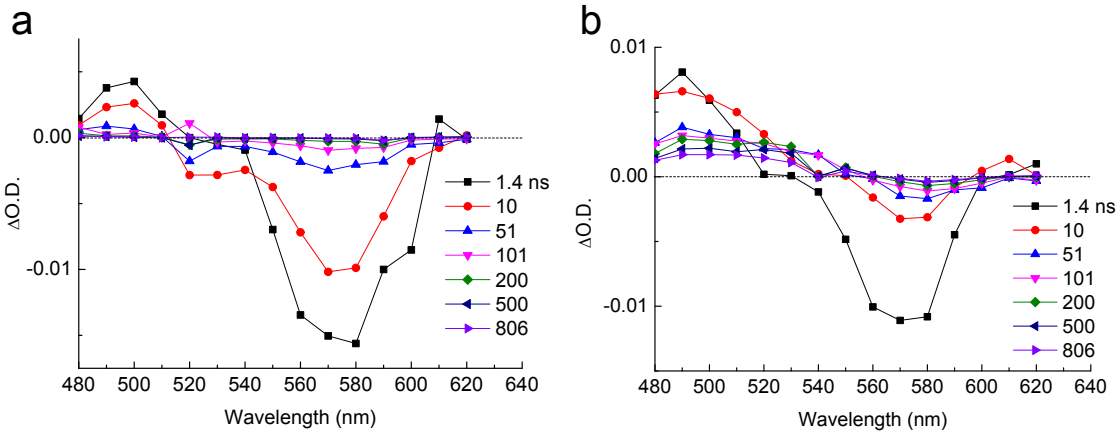

Figure S13. TA spectra of (a) CdTe' and (b) CdTe'-Pe in toluene solution upon excitation by a 590-nm laser.

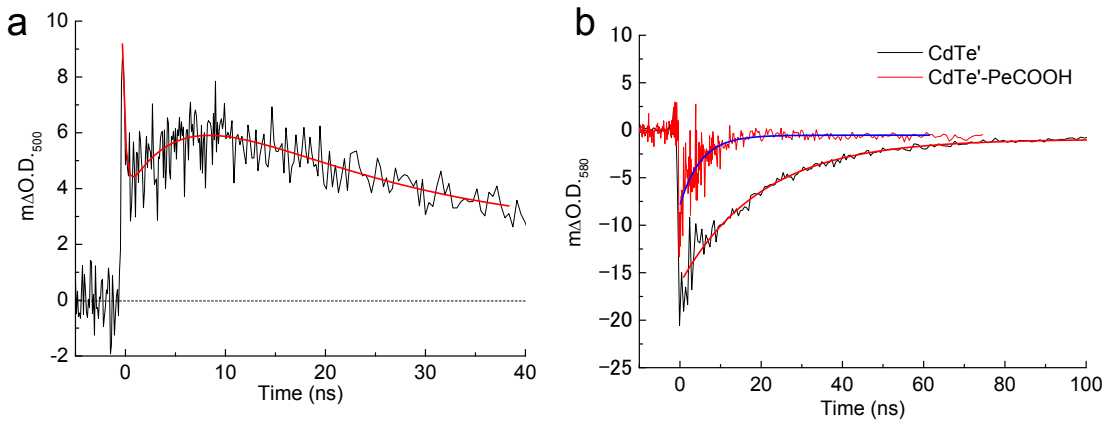

Figure S14. (a) Kinetic profiles at 500 nm used to trace the growth of absorption of Pe (T_1). TTET rate was estimated to be 1.6×10^8 s^{-1}. Solid smooth lines are the best fit. The rise and decay curves were fitted by the following decay function: $y=y_0+A_1\exp(-(x-x_0)/\tau_1)+A_2\exp(-(x-x_0)/\tau_2)-A_3\exp(-(x-x_0)/\tau_3)$. (b) Kinetic profiles at 580 nm used to trace the bleaching and recovery of CdTe'. The TTET rate estimated from the shift of recovery rate between CdTe' and CdTe'-Pe was 1.5×10^8 s^{-1}. Solid smooth lines in red or blue are the best fit. The rise curves were fitted by a single-exponential decay function.

Evaluaton of effect of defects on the estimated recovery rate.

Defect formation during ligand exchange may affect the recovery rate of bleaching of QDs. If the recovery rate is affected by defect formation, then the estimated TTET rate from recovery was also affected by defects. Therefore, it is essential to evaluate the effect of defect formation when the triplet energy transfer rate is estimated from the shift of the recovery rate. To evaluate the effect of defect formation on the recovery rate, we investigated the TTET rate from the growth of TA of Pe (T_1) or shift of recovery rate of CdTe' and CdTe'-Pe (n = 16). Because the growth of TA of Pe (T_1) directly reflects the TTET from CdTe' to Pe, the TTET rate estimated form the growth of Pe (T_1) is the inherent TTET rate. If the TTET rate estimated using the shift of recovery rate was similar to the inherent TTET rate, we can conclude that the effect of defects is negligible.

The TTET rate estimated from the growth of TA of Pe (T_1) was 1.6×10^8 s^{-1}. The TTET rate estimated from the recovery of bleaching of QD was 1.5×10^8 s^{-1}. Therefore, we concluded that the effect of defect formation was negligible in the present experiment. Because the estimation of TTET rate from the growth of TA of Pe (T_1) is almost impossible to measure when the TTET efficiency is low, determining TTET rate from the shift of recovery rate is a powerful strategy to estimate TTET rate in the present experiment.

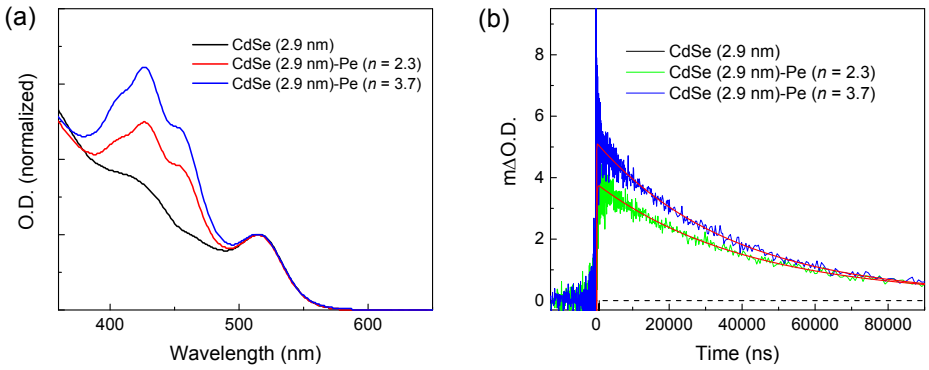

Figure S15. (a) UV-vis spectra of CdSe (2.9 nm) and CdSe (2.9 nm)-Pe. (b) Kinetic profiles at 500 nm of CdSe (2.9 nm)-Pe upon selective excitation at 532 nm (6 μJ per pulse).

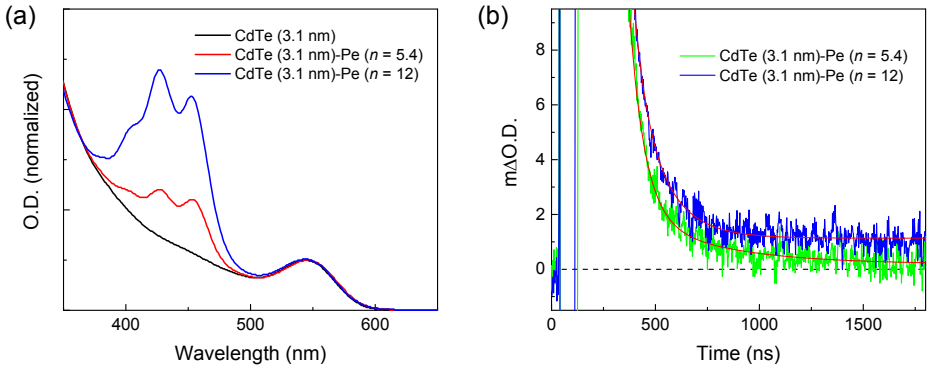

Figure S16. (a) UV-vis spectra of CdTe (3.1 nm) and CdTe (3.1 nm)-Pe. (b) Kinetic profiles at 500 nm of CdSe (3.1 nm)-Pe upon selective excitation at 532 nm (6 μJ per pulse).

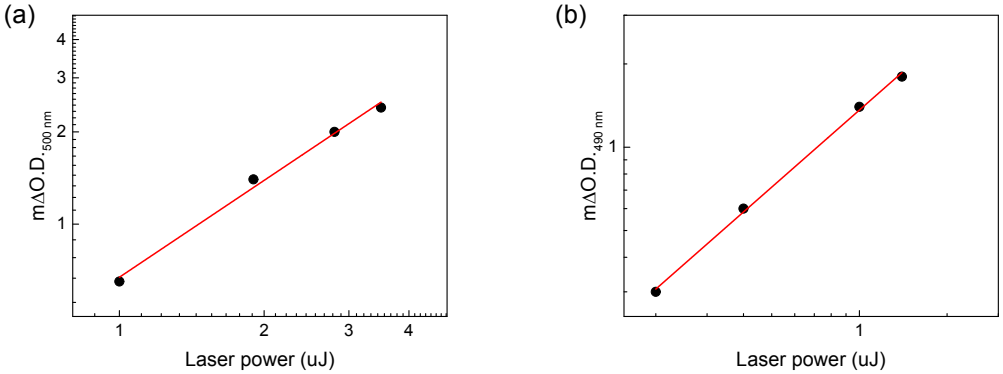

Figure S17. Log-log plots of laser-power dependence of the intensity of transient absorption of Pe (T_1) of CdSe (3.3 nm)-Pe (a) and CdTe (3.4 nm)-Pe (b). The slope is 1, which indicates that the TTET is a one-photon process.

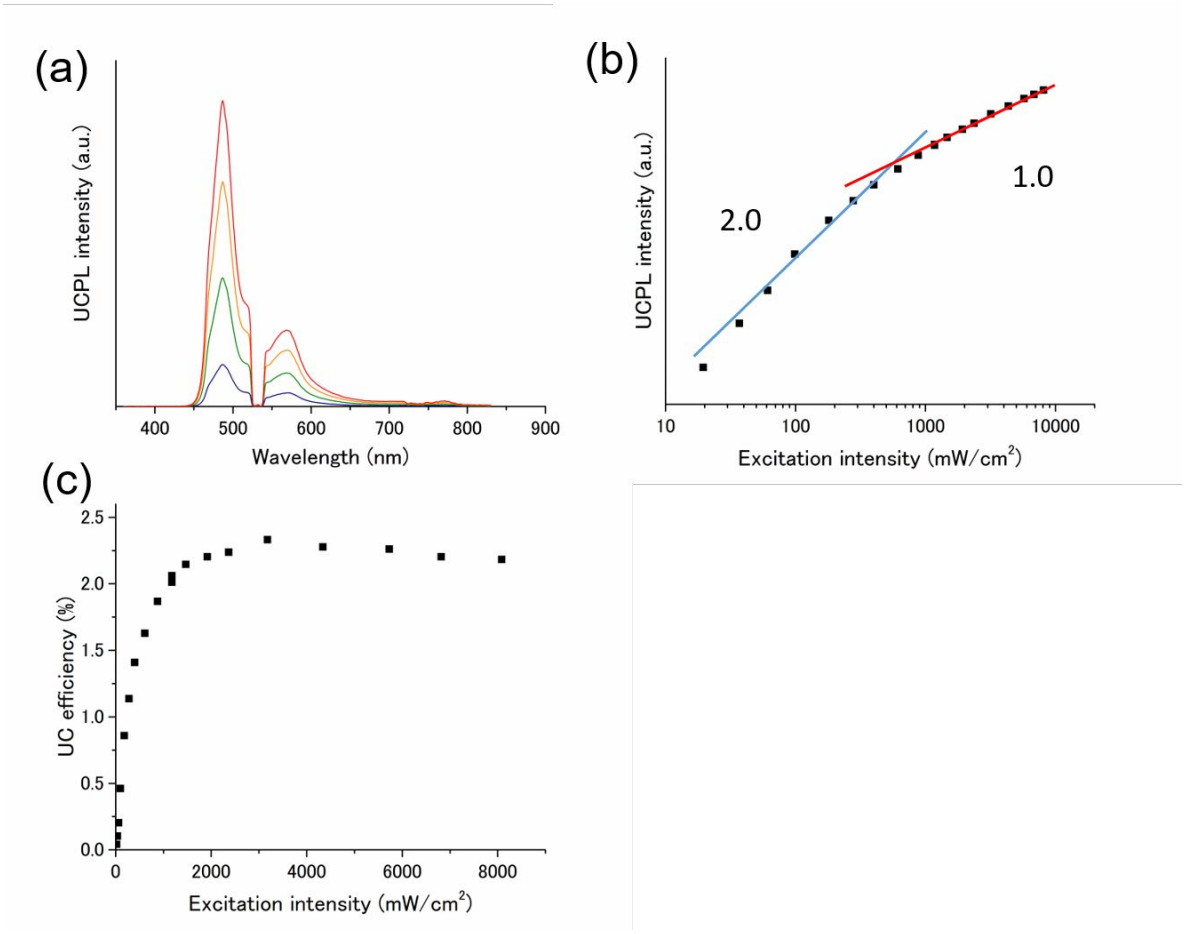

Figure S18. (a) Photoluminescence spectra of CdSe (3.3 nm)-Pe (n = 6.0)-TTBP in deaerated toluene measured at different excitation intensities using a 532-nm laser. A notch filter (λ = 532 nm) were used to remove the scattered incident light. (b) Excitation intensity dependence of the upconversion photoluminescence intensity of CdSe (3.3 nm)-Pe (n = 6.0)-TTBP in deaerated toluene at 487 nm. Blue and red lines show the fitting results with slopes of 2 and 1, respectively. (c) Excitation intensity dependence of TTA-UC efficiency (Φ_{UC}') for CdSe (3.3 nm)-Pe (n = 6.0)-TTBP in deaerated toluene.

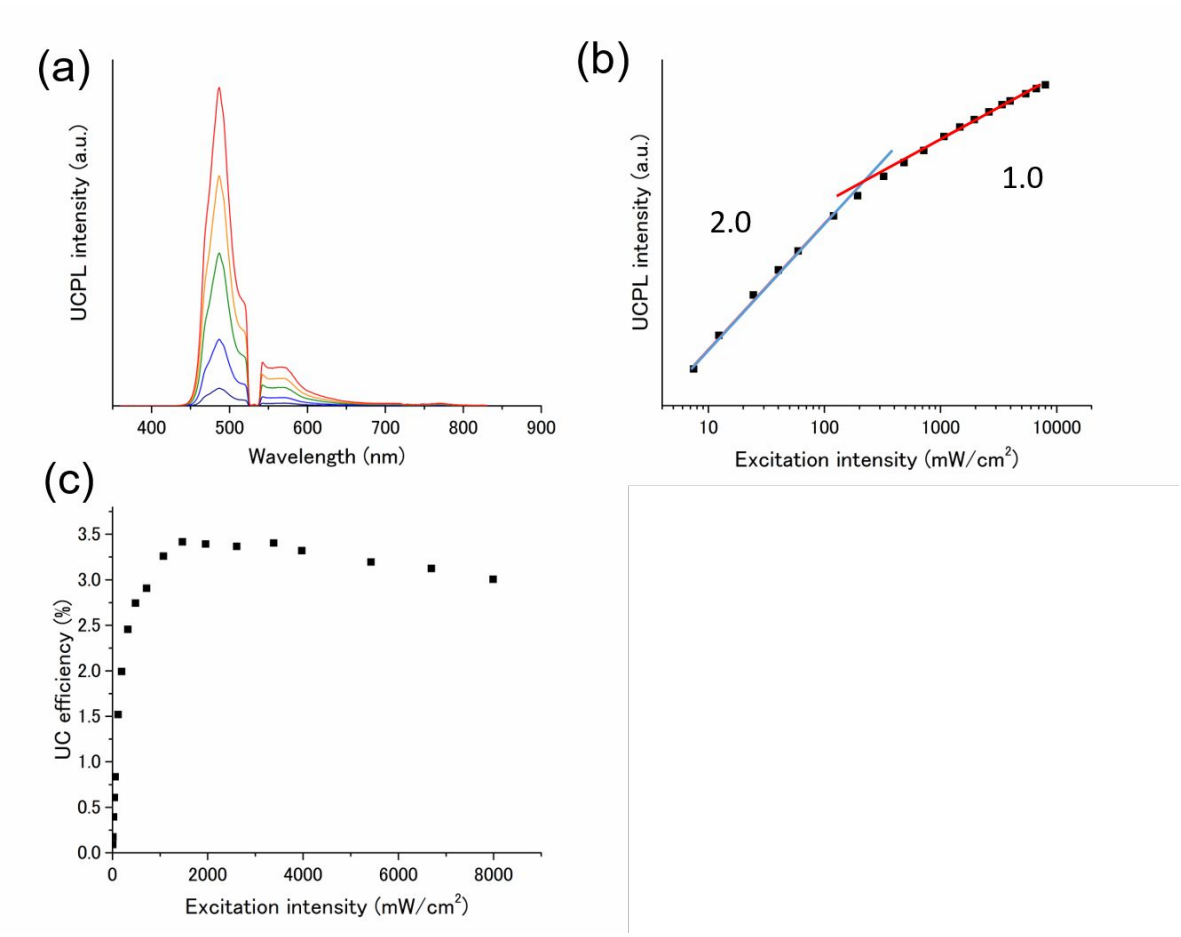

Figure S19. (a) Photoluminescence spectra of CdSe (3.3 nm)-Pe (n = 9.5)-TTBP in deaerated toluene measured at different excitation intensities using a 532-nm laser. A notch filter (λ = 532 nm) were used to remove the scattered incident light. (b) Excitation intensity dependence of the upconversion photoluminescence intensity of CdSe (3.3 nm)-Pe (n = 9.5)-TTBP in deaerated toluene at 487 nm. Blue and red lines show the fitting results with slopes of 2 and 1, respectively. (c) Excitation intensity dependence of TTA-UC efficiency (Φ_{UC}') for CdSe (3.3 nm)-Pe (n = 9.5)-TTBP in deaerated toluene.

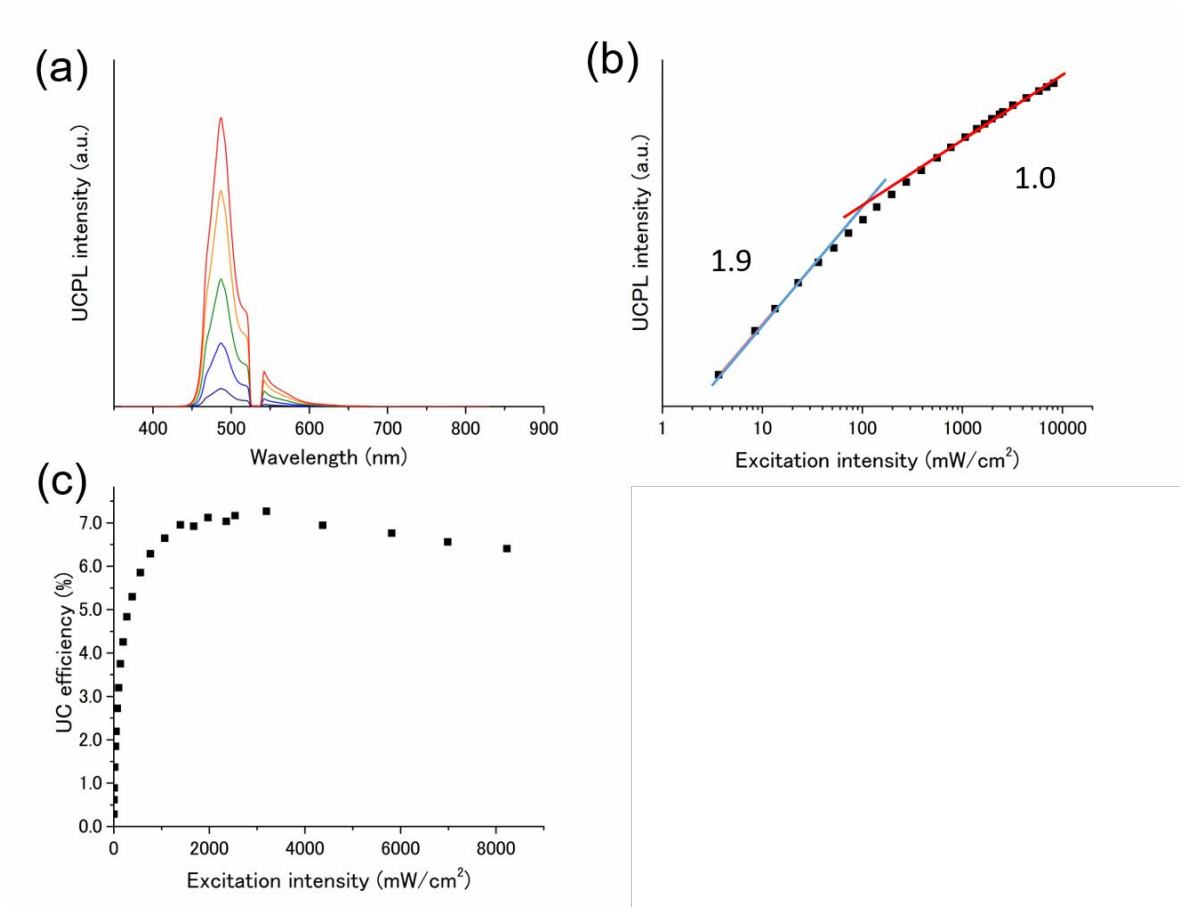

Figure S20. (a) Photoluminescence spectra of CdSe (3.3 nm)-Pe (n = 16)-TTBP in deaerated toluene measured at different excitation intensities using a 532-nm laser. A notch filter (λ = 532 nm) were used to remove the scattered incident light. (b) Excitation intensity dependence of the upconversion photoluminescence intensity of CdSe (3.3 nm)-Pe (n = 16)-TTBP in deaerated toluene at 487 nm. Blue and red lines show the fitting results with slopes of 2 and 1, respectively. (c) Excitation intensity dependence of TTA-UC efficiency (Φ_{UC}') for CdSe (3.3 nm)-Pe (n = 16)-TTBP in deaerated toluene.

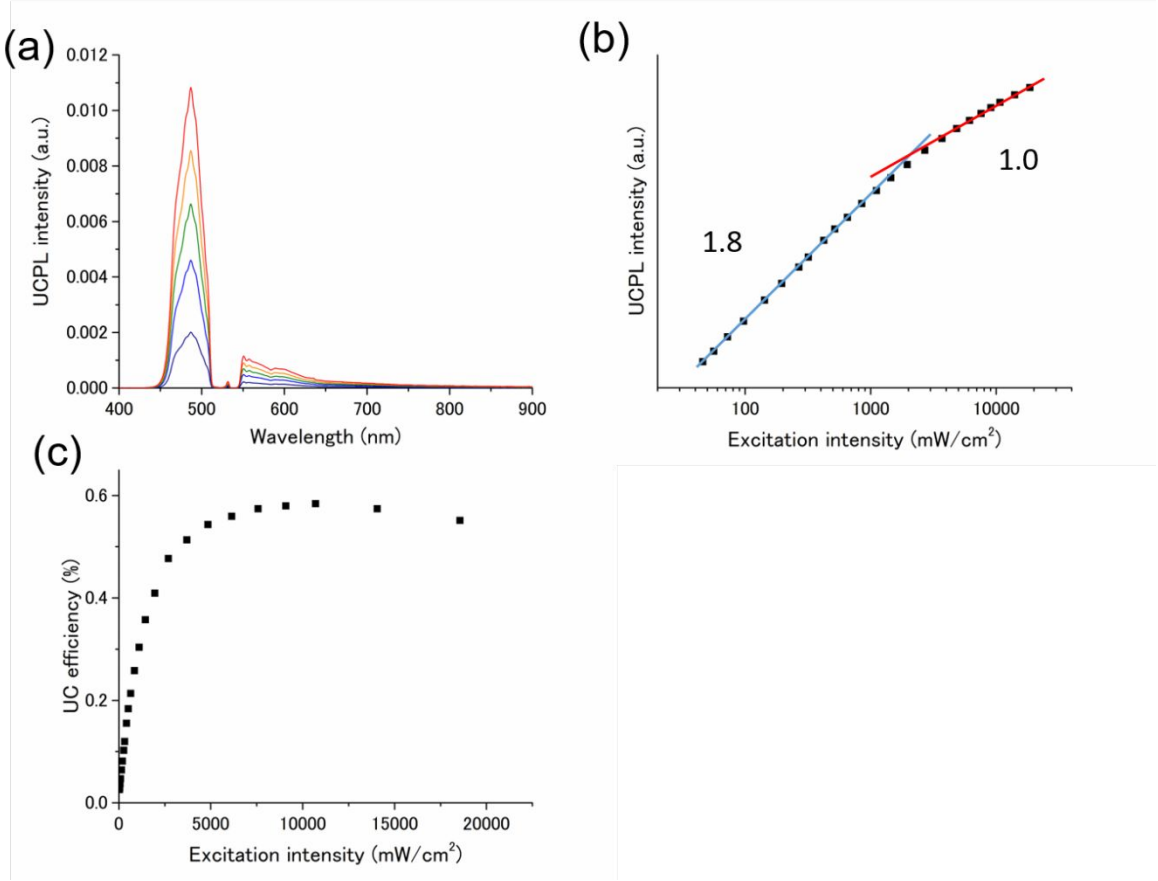

Figure S21. (a) Photoluminescence spectra of CdSe (4.2 nm)-Pe (n = 18)-TTBP in deaerated toluene measured at different excitation intensities using a 532-nm laser. A notch filter (λ = 532 nm) and short-pass filter (λ = 570 nm) were used to remove the scattered incident light. (b) Excitation intensity dependence of the upconversion photoluminescence intensity of CdSe (4.2 nm)-Pe (n = 18)-TTBP in deaerated toluene at 487 nm. Blue and red lines show the fitting results with slopes of 2 and 1, respectively. (c) Excitation intensity dependence of TTA-UC efficiency (Φ_{UC}') for CdSe (4.2 nm)-Pe (n = 18)-TTBP in deaerated toluene.

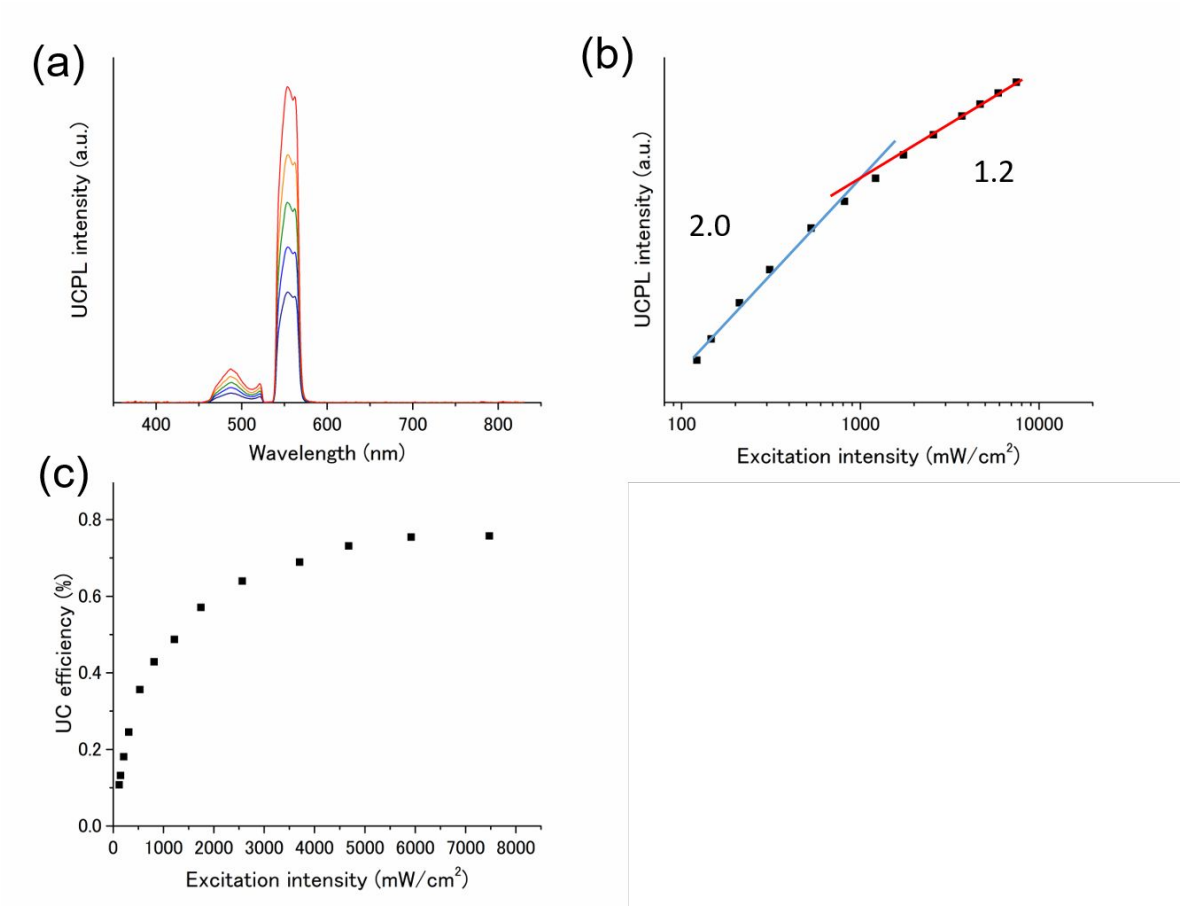

Figure S22. (a) Photoluminescence spectra of CdTe (3.4 nm)-Pe (n = 8.1)-TTBP in deaerated toluene measured at different excitation intensities using a 532-nm laser. A notch filter (λ = 532 nm) and short-pass filter (λ = 570 nm) were used to remove the scattered incident light. (b) Excitation intensity dependence of the upconversion photoluminescence intensity of CdTe (3.4 nm)-Pe (n = 8.1)-TTBP in deaerated toluene at 487 nm. Blue and red lines show the fitting results with slopes of 2 and 1, respectively. (c) Excitation intensity dependence of TTA-UC efficiency (Φ_{UC}') for CdTe (3.4 nm)-Pe (n = 8.1)-TTBP in deaerated toluene.

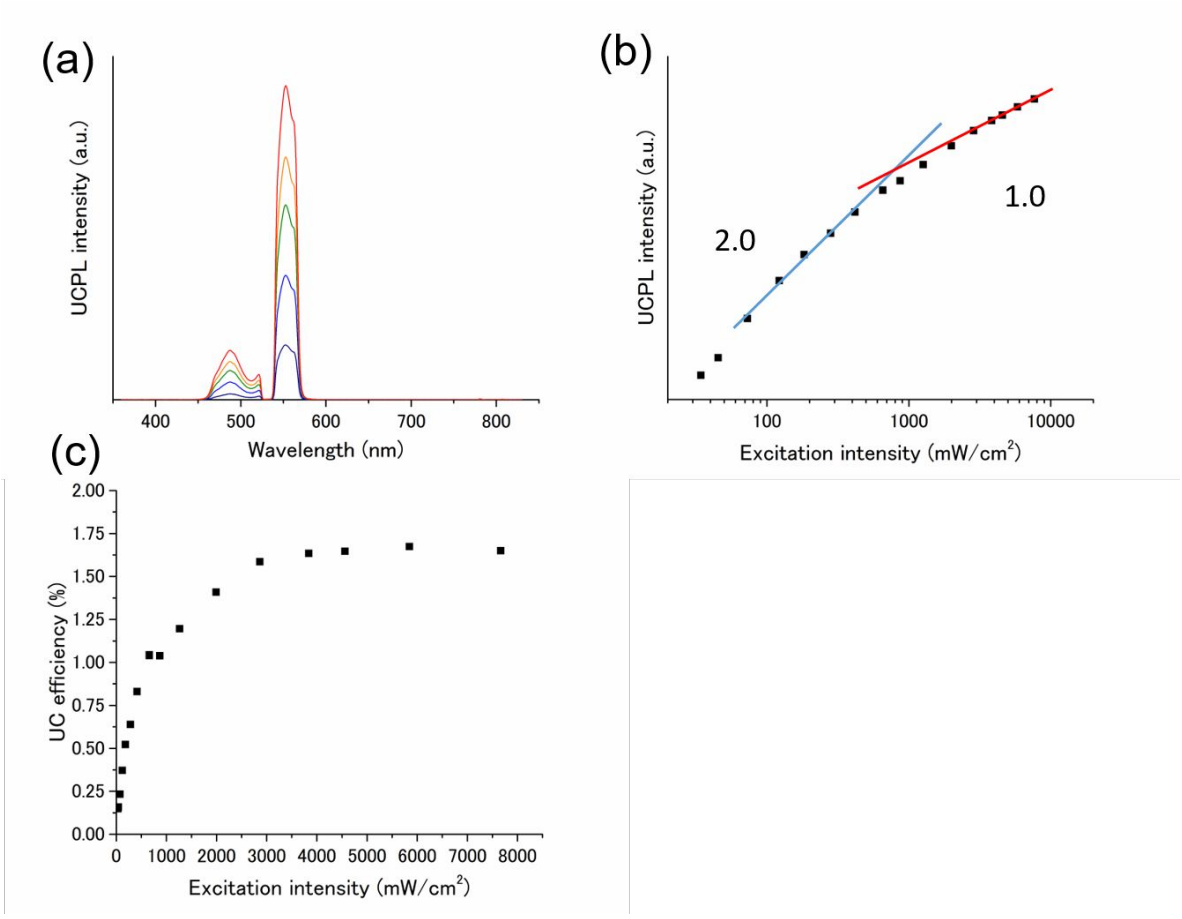

Figure S23. (a) Photoluminescence spectra of CdTe (3.4 nm)-Pe (n = 14)-TTBP in deaerated toluene measured at different excitation intensities using a 532-nm laser. A notch filter (λ = 532 nm) and short-pass filter (λ = 570 nm) were used to remove the scattered incident light. (b) Excitation intensity dependence of the upconversion photoluminescence intensity of CdTe (3.4 nm)-Pe (n = 14)-TTBP in deaerated toluene at 487 nm. Blue and red lines show the fitting results with slopes of 2 and 1, respectively. (c) Excitation intensity dependence of TTA-UC efficiency (Φ_{UC}') for CdTe (3.4 nm)-Pe (n = 14)-TTBP in deaerated toluene.

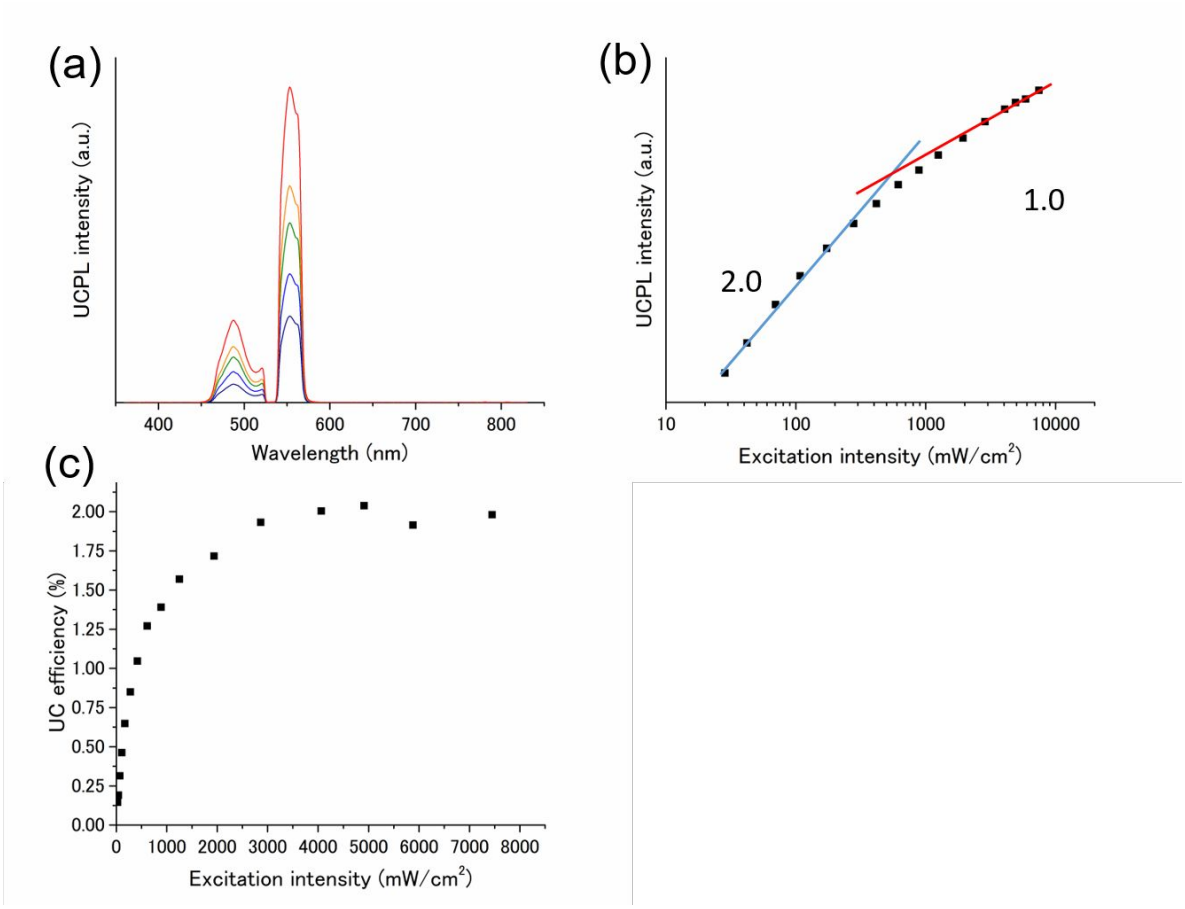

Figure S24. (a) Photoluminescence spectra of CdTe (3.4 nm)-Pe (n = 19)-TTBP in deaerated toluene measured at different excitation intensities using a 532-nm laser. A notch filter (λ = 532 nm) and short-pass filter (λ = 570 nm) were used to remove the scattered incident light. (b) Excitation intensity dependence of the upconversion photoluminescence intensity of CdTe (3.4 nm)-Pe (n = 19)-TTBP in deaerated toluene at 487 nm. Blue and red lines show the fitting results with slopes of 2 and 1, respectively. (c) Excitation intensity dependence of TTA-UC efficiency (Φ_{UC}') for CdTe (3.4 nm)-Pe (n = 19)-TTBP in deaerated toluene.

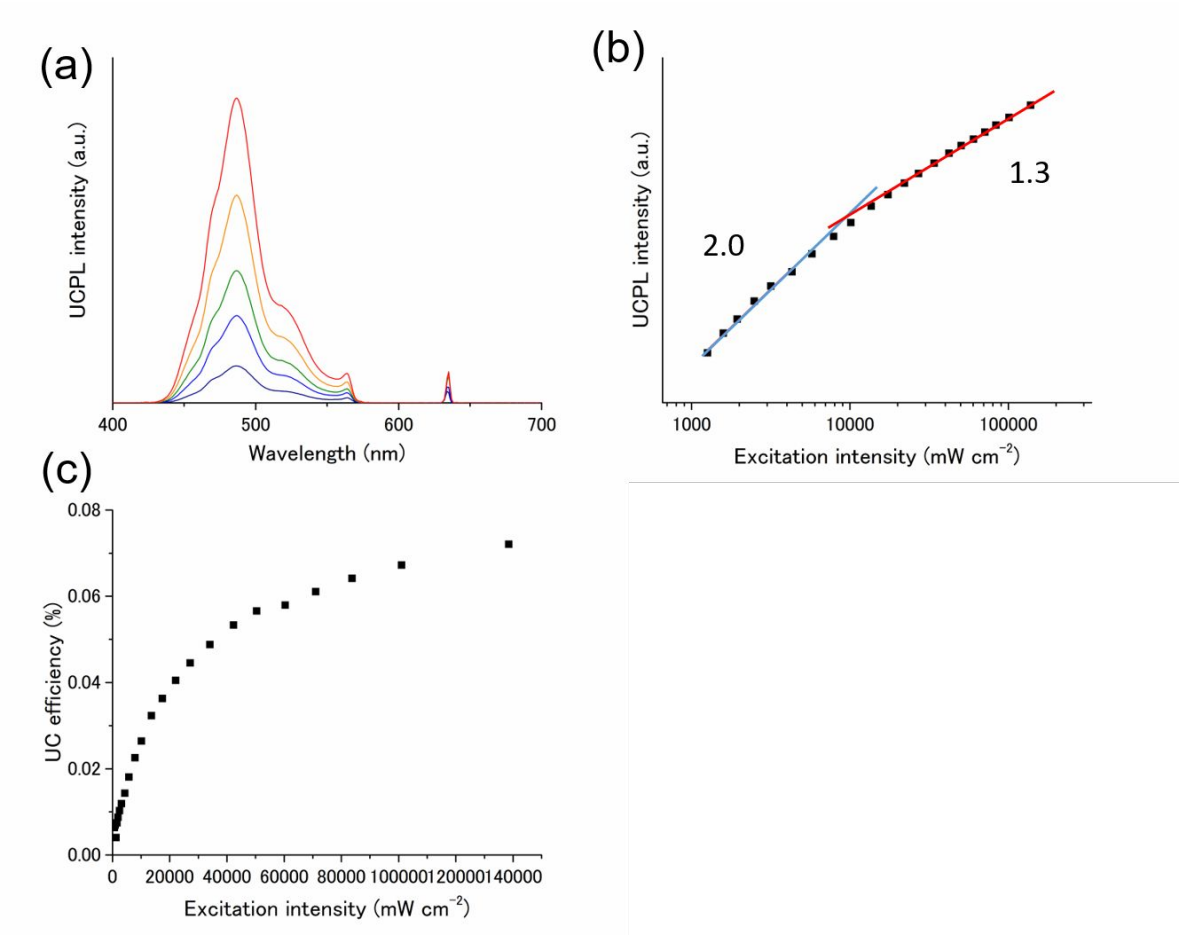

Figure S25. (a) Photoluminescence spectra of CdTe (3.7 nm)-Pe (n = 11)-TTBP in deaerated toluene measured at different excitation intensities using a 635-nm laser. A short-pass filter (λ = 570 nm and 610 nm) was used to remove the scattered incident light. (b) Excitation intensity dependence of the upconversion photoluminescence intensity of CdTe (3.7 nm)-Pe (n = 11)-TTBP in deaerated toluene at 487 nm. Blue and red lines show the fitting results with slopes of 2 and 1, respectively. (c) Excitation intensity dependence of TTA-UC efficiency (Φ_{UC}') for CdTe (3.7 nm)-Pe (n = 18)-TTBP in deaerated toluene.

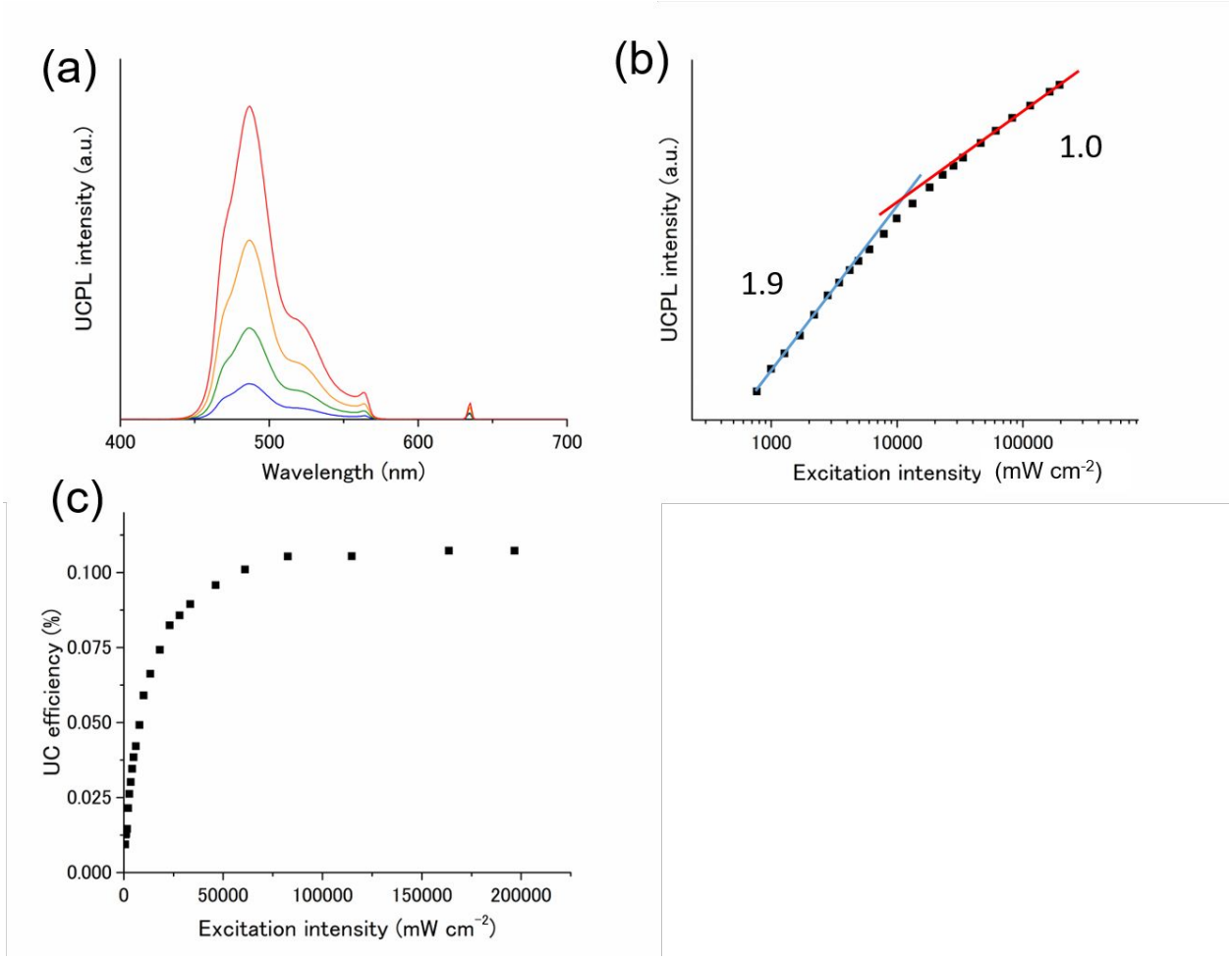

Figure S26. (a) Photoluminescence spectra of CdTe (3.7 nm)-Pe (n = 18)-TTBP in deaerated toluene measured at different excitation intensities using a 635-nm laser. A short-pass filter (λ = 570 and 610 nm) was used to remove the scattered incident light. (b) Excitation intensity dependence of the upconversion photoluminescence intensity of CdTe (3.7 nm)-Pe (n = 18)-TTBP in deaerated toluene at 487 nm. Blue and red lines show the fitting results with slopes of 2 and 1, respectively. (c) Excitation intensity dependence of TTA-UC efficiency (Φ_{UC}') for CdTe (3.7 nm)-Pe (n = 18)-TTBP in deaerated toluene.

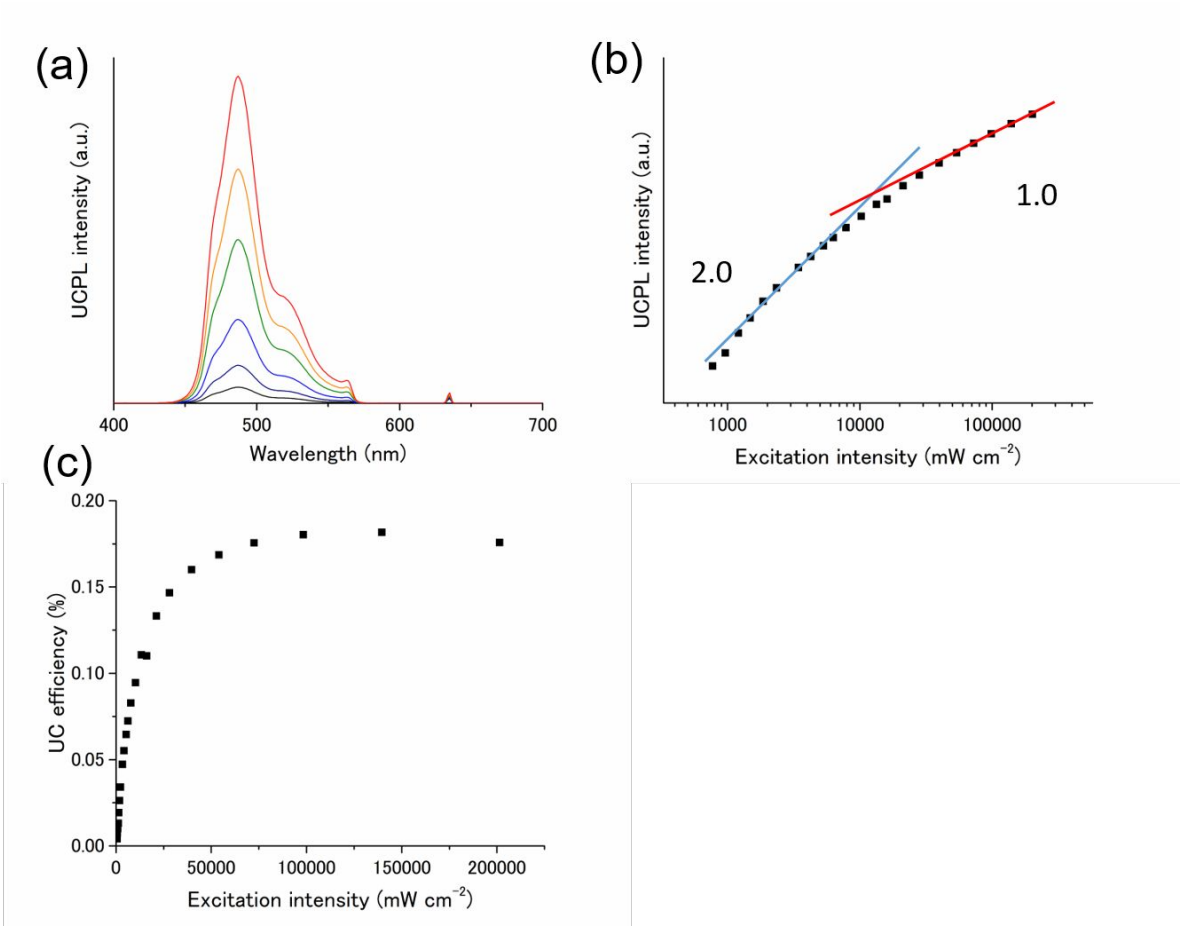

Figure S27. (a) Photoluminescence spectra of CdTe (3.7 nm)-Pe (n = 30)-TTBP in deaerated toluene measured at different excitation intensities using a 635-nm laser. A short-pass filter (λ = 570 and 610 nm) was used to remove the scattered incident light. (b) Excitation intensity dependence of the upconversion photoluminescence intensity of CdTe (3.7 nm)-Pe (n = 30)-TTBP in deaerated toluene at 487 nm. Blue and red lines show the fitting results with slopes of 2 and 1, respectively. (c) Excitation intensity dependence of TTA-UC efficiency (Φ_{UC}') for CdTe (3.7 nm)-Pe (n = 30)-TTBP in deaerated toluene.

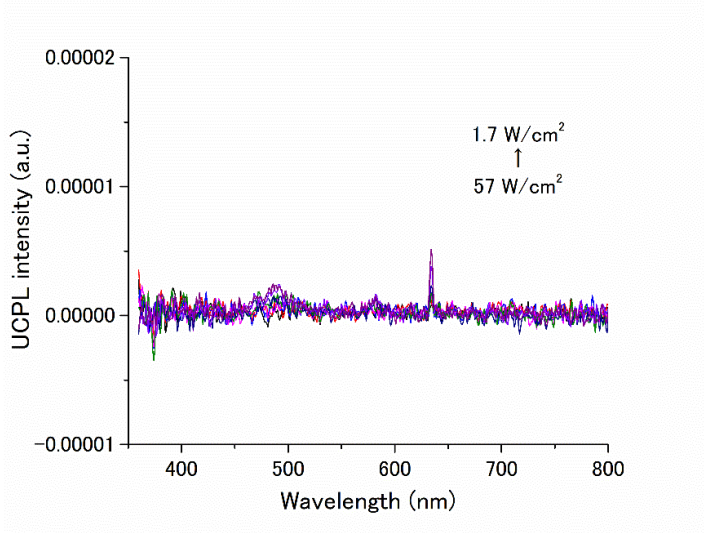

Figure S28. Photoluminescence spectra of CdTe (4.4 nm)-Pe (n = 58)-TTBP in deaerated toluene measured at different excitation intensities using a 635-nm laser. A short-pass filter (λ = 570 and 610 nm) was used to remove the scattered incident light. Weak upconverted emission was observed.

Table S1. TTET Efficiency (Φ_{TTET}), PL Quantum Yield (Φ_{PL}), and Photon Upconversion Efficiency (Φ_{UC}).

Sample	n	Φ_{TTET} [%]	Φ_{PL} [%]	Φ_{UC} [%]
CdSe (3.3 nm)-Pe	0.0	N/A*	4.9	NA
	6.0	18.9	0.1	2.0
	9.5	28.5	0.0	3.4
	16	47.2	0.0	7.0
CdSe (4.2 nm)-Pe	0.0	N/A*	2.8	NA
	9.3	8.03	0.0	NA
	18	11.4	0.0	0.56
	38	15.7	0.0	0.52
CdSe (5.2 nm)-Pe	64	0	NA	NA
CdTe (3.4 nm)-Pe	0.0	NA	36	NA
	8.1	9.12	14	0.70
	14	16.8	9.0	1.5
	19	25.6	7.5	2.0
CdTe (3.7 nm)-Pe	0.0	N/A*	23	NA
	11	3.37	5.7	0.070
	18	4.67	6.2	0.11
	30	7.51	5.6	0.18
CdTe (4.4 nm)-Pe	58	0	NA	NA

N/A*: no energy transfer occurred.

REFERENCES

1. Yu, W. W.; Qu, L. H.; Guo, W. Z.; Peng, X. G., Experimental Determination of the Extinction Coefficient of CdTe, CdSe, and CdS Nanocrystals. *Chem. Mater.* **2003**, 15, 2854-2860
2. Bensasson, R.; Land, E. J., Triplet-Triplet Extinction Coefficients via Energy Transfer. *Trans. Faraday Soc.* **1971**, 67, 1904-1915.
3. Mongin, C.; Moroz, P.; Zamkov, M.; Castellano, F. N., Thermally Activated Delayed Photoluminescence From Pyrenyl-Functionalized CdSe Quantum Dots. *Nat. Chem.* **2018**, 10, 225-230.
4. La Rosa, M.; Denisov, S. A.; Jonusauskas, G.; McClenaghan, N. D.; Credi, A., Designed Long-Lived Emission from CdSe Quantum Dots through Reversible Electronic Energy Transfer with a Surface-Bound Chromophore. *Angew. Chem. Int. Ed.* **2018**, 57, 3104-3107.